Available online at www.sciencedirect.com
ScienceDirect
Solid State Nuclear Magnetic Resonance 31 (2007) 1–9
Solid State Nuclear Magnetic Resonance
www.elsevier.com/locate/ssnmr

Comparison of high-resolution solid-state NMR MQMAS and STMAS methods for half-integer quadrupolar nuclei

Julien Trebosc[a], Jean-Paul Amoureux[a,*], Zhehong Gan[b]

[a]*UCCS, CNRS-8181, University of Lille-1, C7-ENSCL, 59652 Villeneuve d'Ascq, France*
[b]*NHMFL, 32310 Tallahassee, FL, USA*

Received 15 May 2006; received in revised form 18 September 2006
Available online 28 September 2006

Abstract

Several different amplitude-modulated two-dimensional high-resolution methods, based on MQMAS and STMAS, are compared. They include 3QMAS, 5QMAS, DQ-STMAS, and DQF-STMAS experiments. A new method, called t_1-split-STMAS, is also proposed for spin-3/2 nuclei. The comparison is performed in terms of isotropic resolution and spectral-width, efficiency, and sensitivity to magic-angle offset and spinning speed fluctuations.

1. Introduction

Nuclear magnetic resonance (NMR) is one of the most powerful tools available to the community of researchers in various areas of physics, chemistry, materials science, biology and medicine. NMR's ability to probe the structure of materials at atomic level strongly depends upon the availability of high-resolution spectra. In solution, isotropic molecular tumbling averages all anisotropic spin interactions, yielding high-resolution spectra. In the solid state without this rapid averaging, various anisotropic interactions remain and broaden the spectra of static powder samples, and render NMR more difficult for structural determinations. The resolution and sensitivity gaps between liquid and solid state NMR began to decrease in the 1960s with the introduction of radio frequency (RF) decoupling [1], and magic angle spinning (MAS) [2].

Until recently, however, these techniques could not overcome the line broadening in NMR spectra of spin $S>1/2$ rising from the quadrupolar coupling.

This interaction between non-spherical electrical charge distribution of nuclear spins greater than 1/2 and the gradients of the electric field created by the surrounding electrons is typically much larger than dipolar couplings and chemical shift anisotropies. Even with the $(1/2\leftrightarrow-1/2)$ central transition (CT) of half-integer spin that is not submitted to first-order quadrupole interaction, the second-order quadrupolar effect is still the dominant cause of line broadening, even under MAS. Indeed, this second-order effect contains anisotropic terms of ranks 2 and 4, the latter being only partly averaged under MAS rotation. The observation of high-resolution spectra of half-integer quadrupolar spins became possible with the use of the one-dimensional (1D) double rotation (DOR) and two-dimensional (2D) dynamic angle spinning (DAS) [3,4] experiments. Both techniques are based on the manipulation of the spatial part of the quadrupolar Hamiltonian by rendering the position of the rotation axis time-dependent. However, the technical challenge posed by DOR and the limitations of DAS in dealing with strong dipolar couplings or fast relaxing systems have limited the routine use of these techniques. The observation of quadrupolar nuclei with half-integer spin got a significant boost in 1995, with the introduction of the 2D multiple-quantum MAS (MQMAS) method that correlates the multiple-quantum transition during the evolution time t_1 with the CT during the observation time t_2 [5]. A complementary technique was proposed in 2000 with the introduction of the 2D satellite-transition (ST) MAS (STMAS) method, which correlates the single-quantum (SQ) inner-satellite

*Corresponding author. Fax: +33 3 20 43 68 14.
E-mail address: jean-paul.amoureux@univ-lille1.fr (J.-P. Amoureux).

0926-2040/$ - see front matter © 2006 Published by Elsevier Inc.
doi:10.1016/j.ssnmr.2006.09.002

transitions (ST) during t_1 with the CT during t_2 [6]. For all crystallites, the three 2D methods (DAS, MQMAS and STMAS) utilize mirror images during t_1 and t_2, which refocus the second-order quadrupole dephasings along a unique axis, thus leading to observation of high-resolution 2D spectra. Recently, the use of double-quantum (DQ) ST coherences was introduced with the STMAS method. With a CT selective soft π pulse, SQ inner-STs can be transferred efficiently to DQ STs and vice versa. The experiment was originally developed for suppressing undesired CT–CT diagonal peaks by double-quantum filtering (DQF) [7]. Two options are available depending on where to put the t_1 period, with SQ or DQ evolution, namely DQF-STMAS and DQ-STMAS [7]. Both experiments yield high resolution spectra and their isotropic peak positions are identical in a unified representation [8,9]. In this article, we would like to compare the important aspects of efficiencies, resolutions, isotropic spectral widths, and sensitivities to spinning speed fluctuations and magic-angle offset between the two methods, along with MQMAS. We also propose a hybrid version of DQ-STMAS and DQF-STMAS, called t_1-split-STMAS, for obtaining a simultaneous refocusing of signals arising through both symmetrical pathways used during t_1 in an amplitude-modulated experiment.

2. Mathematical description

2.1. Quadrupole frequency

Under fast spinning speed, the quadrupole frequency between Zeeman states m and n of the p-quantum (pQ: $p = n–m$) level coherence, can be written as [10–12]

$$\nu_{m,n} = \nu^1_{m,n} + \nu^2_{m,n} + \nu^3_{m,n} + \cdots, \tag{1}$$

where $\nu^1_{m,n}$, $\nu^2_{m,n}$, and $\nu^3_{m,n}$ are the first-, second-, and third-order associated quadrupole frequencies, respectively:

$$\nu^1_{m,n} = \nu_Q(m^2 - n^2)\{3\cos^2\beta_R - 1 + \eta_Q \sin^2\beta_R \cos 2\alpha_R\} d^2_{00}(\chi)/4, \tag{2}$$

$$\nu^2_{m,n} = \nu^2_Q/5040\nu_0 \sum_{l=0,2,4} B_l(\alpha_R,\beta_R,\eta_Q) C_l(S,m,n) d^l_{00}(\chi), \tag{3}$$

$$\nu^3_{m,n} = \nu^3_Q/27\nu^2_0 \sum_{l=0,2,4,6} D_l(\alpha_R,\beta_R,\eta_Q) E_l(S,m^2,n^2) d^l_{00}(\chi), \tag{4}$$

where S is the spin value, ν_0 the Larmor frequency, $\nu_Q = 3C_Q/2S(2S-1)$ the quadrupole frequency, $C_Q = e^2qQ$ the quadrupole coupling constant, η_Q the quadrupole asymmetry parameter, χ the angle between the rotation axis and the magnetic field, and $d^2_{00}(\chi)$, $d^4_{00}(\chi)$ and $d^6_{00}(\chi)$ the Legendre polynomials of order 2, 4 and 6, respectively ($d^0_{00}(\chi) = 1$):

$$d^2_{00}(\chi) = (3\cos^2\chi - 1)/2,$$

$$d^4_{00}(\chi) = (35\cos^4\chi - 30\cos^2\chi + 3)/8,$$

$$d^6_{00}(\chi) = (231\cos^6\chi - 315\cos^4\chi + 105\cos^2\chi - 5)/16, \tag{5}$$

with

$$B_0(\eta_Q) = -56(3 + \eta^2_Q/3), \tag{6}$$

$$B_2(\alpha_R,\beta_R,\eta_Q) = B^2_0 d^2_{00}(\beta_R) + 2B^2_2 \cos 2\alpha_R d^2_{20}(\beta_R), \tag{7}$$

$$B_4(\alpha_R,\beta_R,\eta_Q) = B^4_0 d^4_{00}(\beta_R) + 2B^4_2 \cos 2\alpha_R d^4_{20}(\beta_R) + 2B^4_4 \cos 4\alpha_R d^4_{40}(\beta_R), \tag{8}$$

$$B^2_0 = 20(\eta^2_Q - 3); \quad B^2_2 = 20\eta_Q\sqrt{6}; \quad B^4_0 = 2(18 + \eta^2_Q); \quad B^4_2 = 6\eta_Q\sqrt{10}; \quad B^4_4 = \eta^2_Q\sqrt{70}, \tag{9}$$

with

$$C_l(S,m,n) = C_l(S,m) - C_l(S,n) \quad \text{and}$$

$$E_l(S,m^2,n^2) = E_l(S,m^2) - E_l(S,n^2), \tag{10}$$

$$C_0(S,m) = m[S(S+1) - 3m^2], \tag{11}$$

$$C_2(S,m) = m[8S(S+1) - 12m^2 - 3], \tag{12}$$

$$C_4(S,m) = m[18S(S+1) - 34m^2 - 5], \tag{13}$$

with

$$D_l(\alpha_R,\beta_R,\eta_Q) = c_{l0}(\eta_Q) d^l_{00}(\beta_R) + 2\sum_{k=2,4,\ldots,l} c_{lk}(\eta_Q)\cos k\alpha_R d^l_{k0}(\beta_R), \tag{14}$$

$$E_l(S,m^2) = a_l p_a(S,m^2) + b_l p_b(S,m^2) + c_l p_c(S,m^2) \tag{15}$$

(α_R, β_R) polar angles describe the rotation axis with respect to the quadrupole interaction, and $d^l_{k0}(\beta_R)$ are reduced Wigner matrices of order l, respectively. Parameters a_l, b_l, c_l, and $c_{lk}(\eta_Q)$, as well as p_a, p_b, and p_c even functions of the m Zeeman state have been defined in [12].

2.2. High-resolution 2D methods

Actually, most of the high-resolution experiments are performed under MAS. This means that, in case of small or medium quadrupole interactions, only zeroth- and fourth-rank contributions of the second-order quadrupole interactions (terms with $l = 0$, 4 in Eq. (3)) are then involved in the quadrupole frequency. Moreover, most of the times, only CT signal is used during the acquisition period, and this is the case of all MQ/ST-MAS methods. Their 2D high-resolution spectra, can thus be obtained by selecting during t_1 coherences that cancel simultaneously for all crystallites, at $t_{2e} = Rt_1$, the second-order CT quadrupole anisotropic dephasing that occurs during observation. This canceling is always possible as long as the coherence selected during t_1 presents a $C_4(S, m, n)$ term of opposite sign with respect to that of the CT ($-1Q$: $m = -n = 1/2$):

$$R = -C_4(S,m,n)/C_4(S,1/2,-1/2) > 0. \tag{16}$$

In MQMAS, symmetrical Zeeman states ($m = -n = \pm 3/2, \pm 5/2, \pm 7/2$, or $\pm 9/2$), are used [8]. In STMAS, there are many possible non-symmetrical (m, n) ST couples [13]. However, for sensitivity reasons, only the inner-satellite transitions are actually used: either on the first (St_{1Q}: $\pm 1/2 \leftrightarrow \pm 3/2$) or on the second ($St_{2Q}$: $\pm 1/2 \leftrightarrow \mp 3/2$) quantum levels, leading to the DQF- (Fig. 1a) and DQ- (Fig. 1b) STMAS methods, respectively [7]. The quantum level pQ for the echo-pathway, the slope of the refocusing axis (Eq. (16)), and the corresponding $C_0(S, m, n)/C_0(S, 1/2, -1/2)$ and $C_2(S, m, n)/C_2(S, 1/2, -1/2)$ ratios, are given in Table 1, for the St_{1Q}, and St_{2Q} coherences.

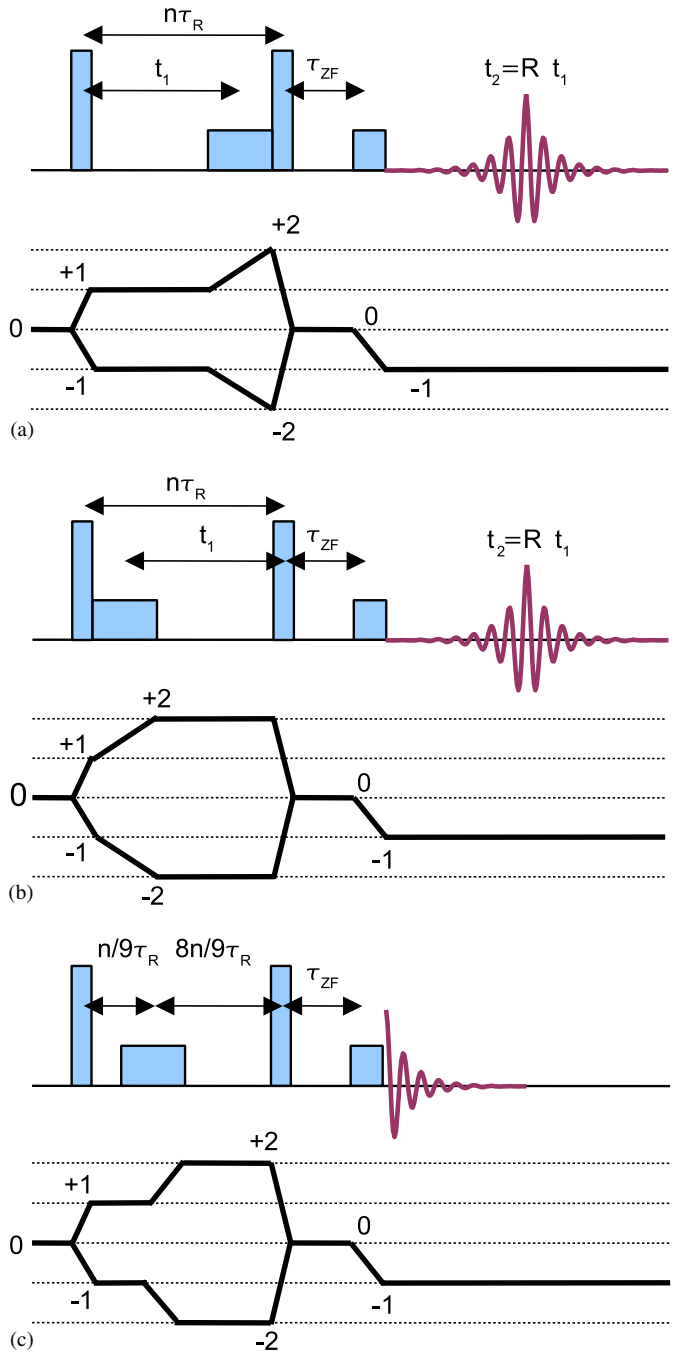

Fig. 1. Four-pulse sequences and coherence transfer pathways corresponding to (a) DQF-STMAS, (b) DQ-STMAS, and (c) t_1-split-STMAS.

It can be observed in Table 1, that the quantum levels of the echo pathways have opposite signs for spin 3/2 nuclei: $-1Q$ and $+2Q$ for DQF-STMAS and DQ-STMAS, respectively. This particularity can be used to obtain the t_1-split-STMAS method described in Fig. (1c). In this method, the magnetization spends 1/9th of the evolution time on $\pm 1Q$ levels, and 8/9th on $\pm 2Q$ levels.

Therefore, the second-order quadrupolar dephasings are thus completely cancelled after t_1, and the two pathways lead simultaneously to an echo at $t_2 = 0$. In DQF-(Fig. 1a), DQ-(Fig. 1b) and t_1-split-(Fig. 1c) STMAS methods, the transfer in between St_{1Q} and St_{2Q} is performed with a soft CT-selective π pulse, called DQF, which also inverts the CT magnetization ($1Q \leftrightarrow -1Q$), and does not affect outer-satellite $1Q$ coherences of spin 5/2, 7/2, and 9/2 [7]. In the case of DQ-STMAS experiments performed on spin-3/2 nuclei, the initial $0Q \rightarrow 2Q$ transfer can also be performed with a single strong hard-pulse. However, this direct $0Q \rightarrow 2Q$ transfer can not be used for larger spin values, due to the multiplicity of ST coherences then encountered on $2Q$ levels, which should lead to several resonances for each sites. Moreover, the efficiency of this direct $0Q \rightarrow 2Q$ transfer is approximately 2–3 times smaller than that observed with the indirect one (Fig. 1b). Eqs. (1)–(15) also apply to the case of nuclei with integer spin values. Unfortunately, in the case of spin-1 nuclei, the three $C_l(S, m, n)$ ($l = 0,2,4$) terms describing second-order quadrupole contributions (Eq. (3)), and the chemical shift, present the same scaling factor of 2 with respect to their values on $-1Q$ coherences. As a result, the $0Q \rightarrow 2Q$ (t_1) $\rightarrow -1Q$ (t_2) high-resolution 2D spectra are completely useless, as the resonances of all species then overlap.

2.3. Universal ppm scaling

Several 2D MAS methods have been proposed to observe high-resolution spectra of half-integer quadrupolar nuclei: 3QMAS [5], 5QMAS [14], DQ-and DQF-STMAS [7], and now t_1-split-STMAS. In order to compare easily results obtained with these methods, a unified ppm scaling has been introduced for MQMAS [8], and extended to DQF-STMAS [9]. In the sheared spectrum, the isotropic frequency F_{iso} can be conveniently expressed as a linear combination of F_1 and F_2,

$$F_{iso} = F_1 + RF_2. \quad (17)$$

In order to introduce the referencing in ppm, let us first consider a single resonance that is not affected by the quadrupole interaction, located at coordinates $(-pv_0\delta_{cs}, v_0\delta_{cs})$ on the un-sheared spectrum. After shearing transformations, its coordinate in the isotropic dimension is

$$F_{iso} = (R - p)v_0\delta_{cs}. \quad (18)$$

Using apparent Larmor frequencies equal to $v_0^{app} = -pv_0$, v_0, and $(R-p)v_0$ along F_1, F_2 and F_{iso}, respectively,

Table 1
Quantum level (p) for the echo pathway, and its refocusing slope $R = t_{2e}/t_1$

S	p_{DQF}	R_{DQF}	C_0^{DQF}/C_0^{CT}	C_2^{DQF}/C_2^{CT}	p_{DQ}	R_{DQ}	C_0^{DQ}/C_0^{CT}	C_2^{DQ}/C_2^{CT}
3/2	−1	8/9	−2	−1/2	+2	1/9	1	−1/2
5/2	+1	7/24	1/8	−7/16	+2	31/24	−7/8	−23/16
7/2	+1	28/45	−2/5	−7/10	+2	73/45	−7/5	−17/10
9/2	+1	55/72	−5/8	−13/16	+2	127/72	−13/8	−29/16

$C_0(S, m, n)/C_0(S, 1/2,-1/2)$ and $C_2(S, m, n)/C_2(S,1/2,-1/2)$ ratios for the echo signal, corresponding to DQF-STMAS ($p = \pm 1$) or DQ-STMAS ($p = 2$) [7].

the ppm scales δ_1, δ_2 and δ_{iso} are all equal to δ_{cs}. It can be shown that, even in the case of nuclei submitted to quadrupole interactions, $v_0^{app} = (R - p)v_0$ allows to obtain for each resonance exactly the same isotropic projection (δ_{iso}), independently of the MQ/ST-MAS method. This means that it always appears at the same place (δ_{iso}, δ_2) in the 2D spectra. It is easy to show that v_0^{app} is identical in DQ-STMAS and DQF-STMAS [9], except for an opposite sign for spin 3/2 nuclei. The same apparent Larmor frequency is also available for the t_1-split-STMAS method, which is a combination of echo and anti-echo signals related to DQ- and DQF-STMAS experiments.

2.4. Isotropic spectral-width and number of t_1 steps

It must be reminded that STs are submitted to first-order quadrupole interactions, that are most of the time much larger than the spinning speed v_R. Therefore, in all STMAS-based methods, this interaction must be cancelled during the evolution time by simultaneously using a perfect magic-angle setting ($\chi_M = 54.736°$), and a perfect t_1 rotor-synchronization (t_1 step equal to $1/v_R$) [6]. In MQMAS methods, it is highly recommended to do the same for three reasons: (i) a small number of t_1 steps are then used, thereby minimizing the acquisition time, (ii) all sidebands are aliased onto the center band, thus maximizing the S/N ratio and simplifying the interpretation of the spectra, and (iii) distortions with respect to MAS spectra are minimized [15]. In case of rotor-synchronized 2D experiments, the indirect sheared spectral-width is equal to $\Delta\delta_{iso} = v_R/(v_0 \cdot |R - p|)$. It can be shown that this spectral-width is identical in the three STMAS methods, and twice and ten times that observed in 3QMAS and 5QMAS [9], respectively. As this spectral-width is inverse proportional to the Larmor frequency, the spinning speed may be insufficient at high magnetic fields, especially with 5QMAS experiments, to cover the frequency range of the various species. STMAS then presents the advantage of wider spectral-width with respect to MQMAS. This problem of the limited isotropic spectral-width can be partially solved by using an alternative representation of the experimental data [16]. First the 2D spectra are sheared with a ratio equal to $|p|$. Such a shearing eliminates the chemical shift along the F_1 dimension. If the peak spread from the quadrupolar shift is within the rotor synchronized window after the shearing, zero-filling can be applied in the F_1 frequency domain. Isotropic spectra can then be obtained by another shearing with a ratio $R-|p|$ of the zero-filled spectra. This procedure solves the aliasing problem when the quadrupolar shift spread is within the spinning frequency [16]. On the other hand, in rotor-synchronized conditions, if we assume inhomogeneous broadening only, the number of t_1 steps required to not truncate the signal is proportional to 1, 5, and 10 in 5QMAS, 3QMAS, and STMAS, respectively [17].

2.5. Isotropic resolution

Let us first define the resolution as the ratio in between the separation of the lines and their line-widths. In order to compare the isotropic resolution, it is thus convenient to use the previous apparent Larmor frequency, as the resonances then always appear at the same positions in the 2D spectra. By doing so, the resolution is therefore directly inverse proportional to the individual isotropic line-widths. In the following, we will only consider the echo pathway, as the anti-echo signal is either not recorded in most full-echo experiments (to decrease the echo delay and hence the signal loss) [18], or only used to cancel the dispersive parts in amplitude-modulated [19] or Echo/Anti-Echo [20,21] experiments. The coherence transfer pathway of the echo-signal of all MQ/ST-MAS amplitude-modulated experiments can always be described in the same way: $0Q \rightarrow pQ\ (t_1) \rightarrow 0Q \rightarrow -1Q\ (\mathrm{CT}, t_2)$ [19]. Let us call T_{CT} and T_p the transverse homogeneous relaxation times of the CT ($-1Q$, t_2) and pQ (t_1) coherences, respectively. These relaxation times, which are related to irreversible processes, can be due either to flip-flop terms or to molecular motions. The 2D signal can be written as

$$s(t_1, t_2) = \exp\left(\mathrm{i}(\omega_p t_1 + \omega_{CT} t_2) - \frac{t_1}{T_p} - \frac{t_2}{T_{CT}}\right). \tag{19}$$

The isotropic signal corresponds to the top of the echo, where all anisotropic terms disappear:

$$s(t_1, Rt_1) = \exp\left\{\mathrm{i}(p - R)v_0\left[\delta_{CS} + \frac{(\delta_{QIS}^{p} + R\delta_{QIS}^{CT})}{p - R}\right] - \frac{1}{T_p} - \frac{R}{T_{CT}}\right\}.t_1, \tag{20}$$

where δ_{cs} and δ_{QIS} are the chemical and quadrupolar-induced shifts, respectively. It has been shown that this

equation can be simplified [8,9]:

$$s(t_1, Rt_1) = \exp\left\{-\mathrm{i}\nu_0^{\mathrm{app}}\delta_{\mathrm{iso}} - \frac{1}{T_{\mathrm{tot}}}\right\}t_1 \quad (21)$$

with

$$\delta_{\mathrm{iso}} = \delta_{\mathrm{cs}} - 10\delta_{\mathrm{QIS}}^{\mathrm{CT}}/17, \quad (22)$$

$$1/T_{\mathrm{tot}} = 1/T_p + R/T_{\mathrm{CT}}. \quad (23)$$

After Fourier and shearing transforms, isotropic projections are thus independent on the 2D high-resolution method, when unified ppm scaling is used, and when only inhomogeneous interactions are taken into account (Eq. (21), without the relaxation term) [8,9]. These interactions may be of different types, such as chemical and quadrupolar-induced shifts, scalar couplings, heteronuclear dipolar interactions, and quadrupolar-dipolar [22] or quadrupolar-CSA [23] cross-terms. In the case of distributed surroundings, such as amorphous samples, these interactions lead to broad resonances. This may be also the case of inhomogeneous static magnetic fields.

In the case of t_1-split-STMAS, both symmetrical pathways have a similar behavior, and the 2D time signal related to one of these pathways can be written as

$$s(t_1, t_2) = \exp\left\{\mathrm{i}\left(\frac{\omega_{1Q} + 8\omega_{2Q}}{9}\,t_1 + \omega_{\mathrm{CT}}t_2\right) - \frac{t_1}{9T_{1Q}} - \frac{8t_1}{9T_{2Q}} - \frac{t_2}{T_{\mathrm{CT}}}\right\}. \quad (24)$$

The isotropic spectrum, $s(t_1,0)$, can be written in the same way as Eq. (21), with

$$\nu_0^{\mathrm{app}} = 17\nu_0/9 \quad \text{and} \quad 1/T_{\mathrm{tot}} = 1/9T_{1Q} + 8/9T_{2Q}. \quad (25)$$

A similar mathematical treatment can be applied to split-t_1-MQMAS methods [24]. In any cases, in unified ppm scaling, Eq. (21) leads to a homogeneous broadening (full-width at half-maximum: FWHM), along the isotropic axis equal to [17]

$$B = 10^6/\pi\nu_0^{\mathrm{app}}T_{\mathrm{tot}}. \quad (26)$$

It has been shown experimentally, that all homogeneous relaxation times of quadrupolar nuclei often are of the same order (within a factor of ca. 2–3) [17]. This fact, which remains true in case of hetero-nuclear decoupling, holds as long as the frequencies of molecular motions do not match the quadrupole interactions. Otherwise, the homogeneous STs relaxation times decrease so largely that they can prevent observation of satellite transitions [25]. As a first approximation, we can assume identical values (T) for irreversible decays, thus leading to broadenings equal to (Table 2)

$$B = (1+R)10^6/\pi\nu_0|R-p|T \quad \text{(MQ/ST-MAS)}, \quad (27)$$

$$B = 9.10^6/\pi\nu_0 17T \quad (t_1\text{-split-STMAS}). \quad (28)$$

The first point to notice in Table 2 is that even in the case of identical irreversible decay values, homogeneous broadenings are largely dependent on the method that is used and on the spin value. Indeed, these broadenings are related (Eq. (27)) to quantum-levels involved during t_1 ($1Q$, $2Q$, $3Q$ or $5Q$), and to the total time ($(1+R)t_1$) up to the top of the echo observed during acquisition. As a general tendency, for each method, these broadenings are largely increasing with the spin value. In the case of spin 9/2, this broadening is so important that the isotropic line-width observed in 3QMAS and STMAS, may be larger than that observed on the second-inner STs [26]. By analyzing results given in Table 2, several other conclusions can be drawn. For spin 3/2 nuclei, the best resolution should be observed in 3QMAS, DQ-STMAS, and t_1-split-STMAS. For larger spin values, the best isotropic resolution is always observed with 5QMAS experiments, which unfortunately present a poor sensitivity [27] and a small rotor-synchronized spectral-width [8]. If these two limitations are not acceptable, the best resolution should then be observed in 3QMAS and DQF-STMAS. Unfortunately, STMAS methods are also submitted to three other additional broadenings, related to magic-angle ill-setting, spinning speed instability [28] and third-order quadrupolar frequencies in case of strong quadrupole interactions [12]. The first-order quadrupole interactions are identical on the St_{1Q} and ST_{2Q} coherences. Therefore, the broadenings observed along the isotropic dimension, due to magic-angle ill-setting: $\chi = \chi_{\mathrm{M}} + \Delta\chi$, are identical in the three STMAS methods. The *total* powder line-width of this broadening is, in universal ppm, equal to $AC_Q\Delta\chi(^\circ)/\nu_0$, with $A = 13067$, 10454, 9334, and 8712, for $S = 3/2$, 5/2, 7/2 and 9/2, respectively [9]. The total MAS CT line-width is equal to

Table 2
Homogeneous broadening, in unified ppm scaling, given in $10^6/\pi\nu_0 T$ unit

S	3QMAS	5QMAS	DQF-STMAS	DQ-STMAS	t_1-Split-STMAS
3/2	8/17		17/17	10/17	9/17
5/2	31/17	37/85	31/17	55/17	
7/2	73/17	50/85	73/17	118/17	
9/2	127/17	131/85	127/17	199/17	

When $T = 3$ ms, this leads to a broadening for $10^6/\pi\nu_0 T \approx 1$ ppm (FWHM), if $\nu_0 = 100$ MHz. Values given for 3QMAS and 5QMAS, also apply to 3QMAS and 5QMAS full-echo experiments [18].

$B[C_Q(1+\eta_Q/6)]^2/\nu_0$, with $B = 3/56$, $9/700$, $15/2744$ and $1/336$, for $S = 3/2$, $5/2$, $7/2$ and $9/2$, respectively. Therefore, for a fixed MAS CT line-width with the same η_Q and ν_0 values, the sensitivity to the magic-angle misset increases with the spin value as it is proportional to 1, 1.633, 2.236 and 2.829, for $S = 3/2$, $5/2$, $7/2$ and $9/2$, respectively. For the same reason of identical first-order quadrupole interactions, the broadenings due to spinning speed instability are identical in the three STMAS methods. St_{1Q} and ST_{2Q} coherences are related to the same Zeeman levels: ($m = \pm 3/2$ and $n = \pm 1/2$), and hence same third-order quadrupole frequency $\nu^3_{m,n}$ (Eq. (4): same difference for $E_l(S, m^2) - E_l(S, n^2)$). The three STMAS-based experiment are thus submitted to the same total additional broadening, with respect to MQMAS. In the case of DOR and DAS ($R = -p = 1$ if $\chi = 37.38°$ and $79.19°$), homogeneous broadenings are always equal to $10^6/\pi\nu_0 T$, and are thus smaller than those observed in 3QMAS, DQF-STMAS or DQ-STMAS, for spin values larger than 3/2.

3. Experimental verifications

We have performed experimental verifications on four different samples: $RbNO_3$ (rubidium nitrate), $41Na_2O$–$20.5Al_2O_3$–$38.5P_2O_5$, $AlPO_4$ berlinite, and $AlPO_4$ VPI5. All experiments have been performed on a 9.4T AVANCE-400 Bruker spectrometer, either with a double-channel STMAS probe equipped with a 4 mm rotor, or with a triple-channel STMAS probe equipped with a 3.2 mm rotor.

There are three different rubidium species in $RbNO_3$ [29]. The maximal values of their isotropic projections can be observed at $\delta_{ISO} = -28.6$, -24.6, and -24.0 ppm in Fig. 2. We have first verified that efficiencies of the three STMAS sequences, are identical. This is related to the fact they have identical coherence transfer pathways, as only the times they spend on $1Q$ and $2Q$ levels during t_1 differ. We have measured the homogeneous relaxation times of the various coherences involved in these experiments [17], and obtained 24, 23, 32, and 55 ms, for t_{1Q}, T_{2Q}, T_{3Q}, and T_{CT}, respectively. These relaxation times correspond (Eq. (26)) to homogeneous broadenings of 0.056 (t_1-split-STMAS: Fig. 2b), 0.029 (3QMAS: Fig. 2c), 0.059 (DQ-STMAS: Fig. 2d), 0.074 (DQF-STMAS: Fig. 2e) ppm (FWHM). The relative values of these broadenings are in qualitative agreement with those given in Table 2 in case of identical irreversible decays. These broadenings are very weak due to long relaxation times and small spin values (^{87}Rb: $S = 3/2$); they should be much larger with spin-9/2 nuclei [26].

In addition to homogeneous broadenings, and in contrast to MQMAS, STMAS-based methods are submitted to extra experimental broadenings due to magic-angle ill-setting and spinning speed fluctuations. The fact that all isotropic spectra present the same resolution, means a quasi perfect experimental setting ($\Delta\chi < 0.001°$). We have also verified on this sample that the three STMAS

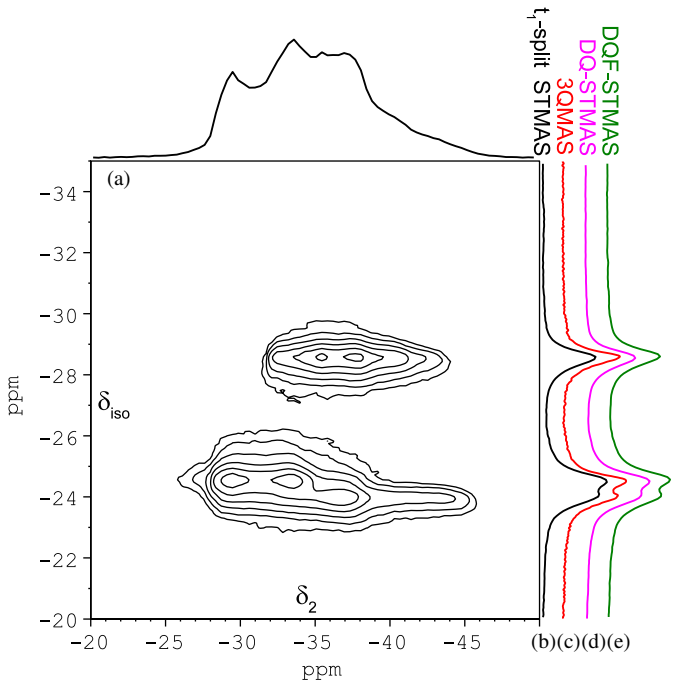

Fig. 2. $RbNO_3$: sheared t_1-split STMAS ^{87}Rb 2D spectrum (a) using the SPAM concept [21], represented in unified ppm scaling, with MAS (top) and isotropic (right) projections. 4 mm rotor, $\nu_R = 12.5$ kHz, RF = 150 and 10 kHz for the hard- and soft-pulses, respectively. Isotropic projections obtained with: t_1-split-STMAS (b), 3QMAS (c), DQ-STMAS (d), DQF-STMAS (e).

methods present the same isotropic spectral width that is twice that observed with t_1-rotor synchronized 3QMAS experiments. For identical experimental specifications the STMAS sensitivity was ca. 5 times larger than with 3QMAS.

Phosphate-based glasses have applications as sealants for electronic applications, as biomaterials, or as encapsulating host matrices for radioactive waste [30]. These applications often benefit from the process of devitrification, which involves the precipitation of crystals after thermal treatment. We have used the $41Na_2O-20.5Al_2O_3$–$38.5P_2O_5$ glass which was devitrified for 6 h at 612 °C. We show its 2D ^{23}Na t_1-split-STMAS spectrum in Fig. 3, with on top its sum projection along δ_{ISO} (a) and the featureless MAS spectrum (b), and on the right the projections along δ_2 of the t_1-split-STMAS (c), DQ-STMAS (d), and DQF-STMAS (e). This sample contains at least 13 different sodium species belonging to several different phases with very different quadrupole interactions. The three 2D spectra (not shown) present all resonances at the same unified ppm (δ_{ISO}, δ_2) positions; however their relative intensities do not represent the correct proportions. The isotropic resolutions (Figs. 3c–e) are again identical due to weak homogeneous broadenings and small spin value (^{23}Na: $S = 3/2$).

$AlPO_4$ berlinite only contains one aluminum species ($C_Q = 4.067$ MHz, $\eta_Q = 0.35$) [28]. In Fig. 4, we have represented the isotropic projection of the 3QMAS (a),

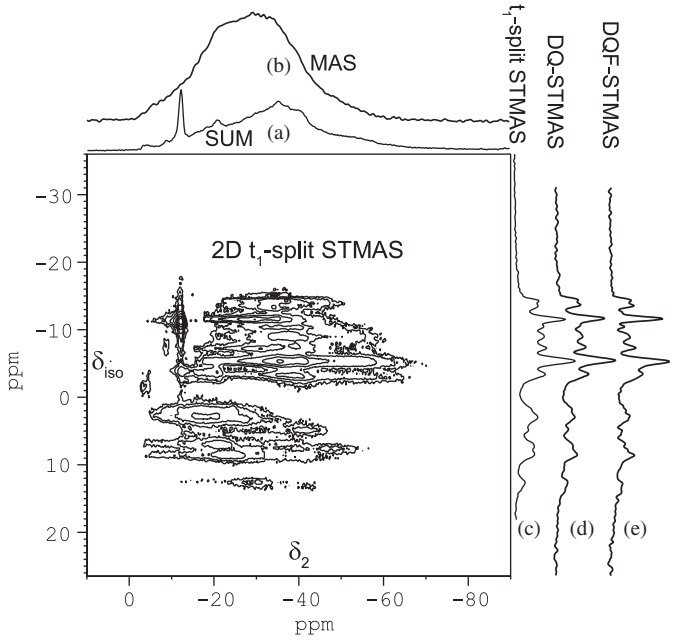

Fig. 3. $41Na_2O–20.5A1_2O_3–38.5P_2O_5$: ^{23}Na t_1-split-STMAS 2D spectrum with on top its sum projection along δ_{iso} (a) and the MAS spectrum (b), and on the right the projections along δ_2 of the t_1-split-STMAS (c), DQ-STMAS (d), and DQF-STMAS (e). A 3.2 mm rotor, $\nu_R = 20$ kHz, RF = 120 and 10 kHz for the hard- and soft-pulses, respectively.

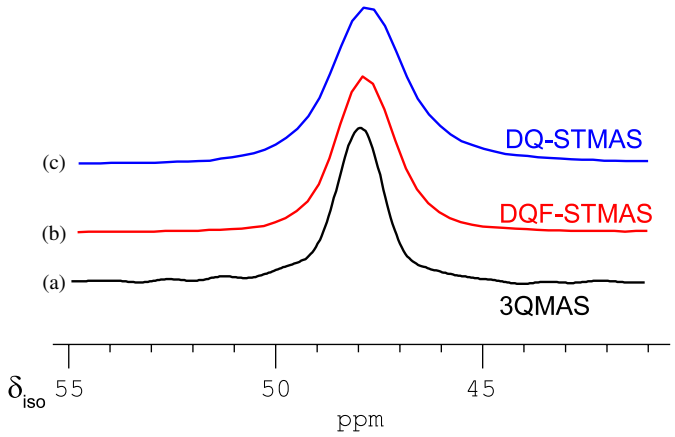

Fig. 4. $AlPO_4$ berlinite: ^{27}Al isotropic projection of the 3QMAS (a), DQF-STMAS (b) and DQ-STMAS (c) 2D sheared spectra. 4 mm rotor, $\nu_R = 12.5$ kHz, RF = 150 and 5 kHz for the hard- and soft-pulses, respectively.

DQF-STMAS (b), and DQ-STMAS (c) 2D sheared spectra. From Table 2, the homogeneous broadening of 3QMAS and DQF-STMAS, should be similar. Therefore, the broader line-width ($\approx$0.3 ppm FWHM) observed in DQF-STMAS, with respect to 3QMAS, is related to spinning speed instability and non-perfect magic-angle setting. By assuming a perfect speed stability, we can obtain a maximum value for the second effect [9]: $\Delta\chi < 0.0015°$. The spinning speed stability and magic-angle setting are identical in DQF-STMAS and DQ-STMAS. Therefore, the isotropic DQF-STMAS line-width should be smaller than that of DQ-STMAS, as can be observed in Figs. 4(b) and (c). We have verified that the rotor-synchronized spectral widths are identical in DQF-STMAS and DQ-STMAS, and twice that of 3QMAS, and that the two STMAS methods present an identical sensitivity to magic-angle ill-setting (Fig. 5) and spinning speed fluctuations. Since pulses and pathways are identical, there is no surprise that we have also measured the same efficiency in all STMAS methods, that is ca. 4 times larger than with 3QMAS.

To finish, we have recorded ^{27}A1 STMAS spectra of hydrated $A1PO_4$ VPI5. This sample contains two tetrahedral and one hexa-coordinated aluminum sites [31]. However, under MAS at 9.4 T, the two tetrahedral sites overlap. Spectral-widths, and efficiencies are identical in DQ-STMAS and DQF-STMAS experiments (not shown). Fig. 6 displays the isotropic projections obtained with

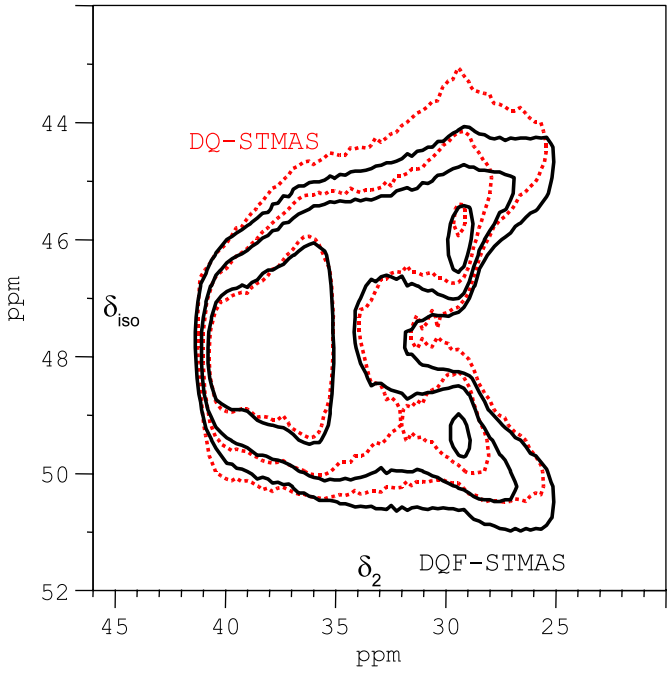

Fig. 5. $A1PO_4$ berlinite: ^{27}Al 2D spectra of DQF-STMAS (continuous lines), and DQ-STMAS (dotted lines), for a not perfectly adjusted magic-angle. Same experimental specifications as in Fig. 4.

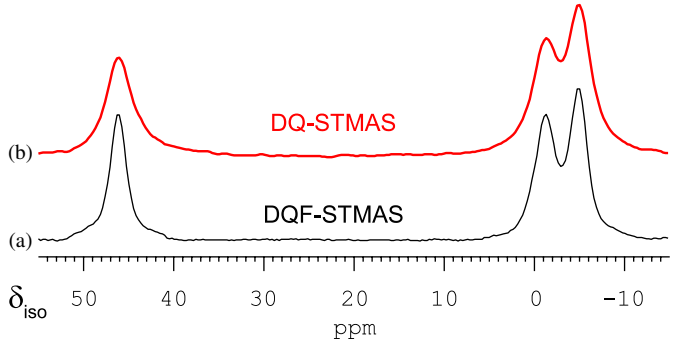

Fig. 6. $AlPO_4$ VPI_5: ^{27}Al isotropic projections of the DQF-STMAS (a), and DQ-STMAS (b) 2D sheared spectra. 4 mm rotor, $\nu_R = 12.5$ kHz, RF = 150 and 5 kHz for the hard- and soft-pulses, respectively. No ^{1}H decoupling.

DQF-STMAS (a), and DQ-STMAS (b), under identical spinning-speed fluctuations and magic-angle setting. As expected from homogeneous broadening values given in Table 2, isotropic resolution is better in DQF-STMAS than in DQ-STMAS.

4. Conclusions

We have analyzed theoretically and compared experimentally two MQMAS (3Q and 5Q) and three STMAS (DQ, DQF, and t_1-split) methods. These methods are complimentary in various aspects. If the main purpose is to get the best possible resolution, 5QMAS should be preferred if homogeneous broadening is the main contribution to the line-width, as its broadening is much smaller than with all other methods. However, its sensitivity and rotor-synchronized isotropic spectral-width are very small, which may lead to long accumulation times. 3QMAS remains the most robust and "general" method, especially in its z-filter [19] and SPAM [20] versions. However, in cases of low sensitivity for nuclei not submitted to molecular motions in the MHz range [25], and if the magic-angle and the spinning speed can be perfectly set up, STMAS then provides much higher sensitivity by 3–5 with slightly less resolution than 3QMAS. As an example, this sensitivity advantage really shows up in case of ^{17}O high-resolution analyses [32,33]. As previously described, all STMAS methods present the same efficiency. However, it must be noted that this efficiency can still be improved by introducing the SPAM (Soft-Pulse Added-Mixing) concept [34], which consists in using all quantum levels in between the last two pulses. This SPAM concept, when applied to DQ-STMAS and DQF-STMAS, allows enhancing the S/N ratio by a factor of ca. 2.8–3 for identical experimental time, with respect to the pulse sequences described in Figs. 1a and b [21]. In the case of t_1-split-STMAS, both symmetrical pathways lead simultaneously to an echo at $t_{2e} = 0$. This means that the same number of rotor-synchronized t_1 steps must be acquired for both pathways with the SPAM echo/anti-echo method, and the S/N is then only enhanced by a factor of ca. 1.4–1.5 with respect to that obtained with the hyper-complex (or TPPI) method using pulse sequence described in Fig. 1c. All STMAS methods present the same isotropic spectral-width, and the same sensitivity to magic-angle setting and spinning speed stability. For homogeneous broadening reasons, DQ-STMAS and t_1-split-STMAS should be preferred for spin 3/2 nuclei and DQF-STMAS for other spin values.

One advantage of t_1-split-STMAS over DQ/DQF-STMAS previous experiments, is in the case of combining it with Q-CPMG sequence [35] for further sensitivity enhancement. Signals coming from both symmetrical pathways always have their maximum values at the same time origin $R = t_{2e} = 0$ and stay stationary while incrementing t_1. Both signals form echoes at the middle of multiple Q-CPMG acquisition windows, thus allowing to shorten the acquisition window. This short delay provides a better S/N ratio than with DQ/DQF-STMAS, where echo and anti-echo signals are going forward and backward versus t_2, respectively, for increasing t_1 values. This leads to longer Q-CPMG pulse intervals and hence larger homo-nuclear attenuation than with t_1-split-STMAS [36]. Phase-cycling corresponding to these sequences should be shortly available on http://rmn800/univ-lille1.fr.

Acknowledgments

Authors would like to thank Region Nord/Pas de Calais, Europe (FEDER), CNRS, French Minister of Science, USTL, ENSCL, and the Bruker company for funding. They would also like to acknowledge Prof. L. Montagne and Drs. G. Tricot and L. Delevoye, for providing the $41Na_2O$–$20.5A1_2O_3$–$38.5P_2O_5$ sample and for the numerous discussions they had together.

References

[1] J.S. Waugh, L.M. Huber, U. Haeberlen, Phys. Lett. 20 (1968) 180; A. Pines, M.G. Gibby, J.S. Waugh, J. Chem. Phys. 56 (1972) 1776.
[2] E.R. Andrew, A. Bradbury, R.G. Eades, Nature (London) 182 (1958) 1659.
[3] A. Samoson, E. Lippmaa, A. Pines, Mol. Phys. 65 (1988) 1013.
[4] A. Llior, J. Virlet, Chem. Phys. Lett. 152 (1998) 248.
[5] L. Frydman, J.S. Harwood, J. Am. Chem. Soc. 117 (1995) 5367–5368.
[6] Z.H. Gan, J. Am. Chem. Soc. 122 (2000) 3242–3243.
[7] H.T. Kwak, Z.H. Gan, J. Magn. Reson. 164 (2003) 369–372.
[8] J.P. Amoureux, C. Fernandez, Solid-State NMR 2 (1993) 83–88; J.P. Amoureux, C. Fernandez, Solid-State NMR 16 (2000) 339–343.
[9] J.P. Amoureux, C. Huguenard, F. Engelke, F. Taulelle, Chem. Phys. Lett. 356 (2002) 497–504.
[10] A. Samoson, Chem. Phys. Lett. 119 (1985) 29–32.
[11] J.P. Amoureux, Solid-State NMR 2 (1993) 83–88.
[12] Z. Gan, P. Srinivasan, J.R. Quine, S. Steuernagel, B. Knott, Chem. Phys. Lett. 367 (2003) 163–169.
[13] S.E. Ashbrook, S. Wimperis, J. Magn. Reson. 156 (2002) 269–281.
[14] C. Fernandez, J.P. Amoureux, Chem. Phys. Lett. 242 (1995) 449–454.
[15] D. Massiot, J. Magn. Reson. A 122 (1996) 240–244.
[16] Z. Gan, in: 45th Rocky Mountain Conference, Denver, USA, July 27–31, 2003.
[17] J.P. Amoureux, J. Trebosc, J. Magn. Reson. 179 (2006) 311–316.
[18] D. Massiot, B. Touzo, D. Trumeau, J.P. Coutures, J. Virlet, P. Florian, P.J. Grandinetti, Solid State NMR 6 (1996) 73–83.
[19] J.P. Amoureux, C. Fernandez, S. Steuernagel, J. Magn. Reson. A 123 (1996) 116–118.
[20] J.P. Amoureux, L. Delevoye, S. Steuernagel, Z. Gan, S. Ganapathy, L. Montagne, J. Magn. Reson. 172 (2005) 268–278.
[21] J.P. Amoureux, L. Delevoye, G. Fink, F. Taulelle, A. Flambard, L. Montagne, J. Magn. Reson. 175 (2005) 285–299.
[22] Z. Gan, D.M. Grant, J. Magn. Reson. 90 (1990) 522–534.
[23] T. Giavani, H. Bildsoe, J. Skibsted, H.J. Jakobsen, J. Magn. Reson. 166 (2004) 262–272.
[24] S.P. Brown, S. Wimperis, J. Magn. Reson. 128 (1997) 42–61.
[25] S.E. Ashbrook, S. Antonijevic, A.J. Berry, S. Wimperis, Chem. Phys. Lett. 364 (2002) 634–642.
[26] J.P. Amoureux, J. Trebosc, J. Magn. Reson. 180 (2006) 311–317.
[27] J.P. Amoureux, C. Fernandez, L. Frydman, Chem. Phys. Lett. 295 (1996) 347–355.
[28] C. Huguenard, F. Taulelle, Z.H. Gan, J. Magn. Reson. 156 (2002) 131–137.

[29] J.H. Baltisberger, S.L. Gam, E.W. Wooten, T.H. Chang, K.T. Mueller, A. Pines, J. Am. Chem. Soc. 114 (1992) 1489–1493.
[30] B.L. Metcalfe, I.W. Donald, J. Non-Cryst. Solids. 348 (2004) 225–229.
[31] L.B. McCuster, C. Baerlocher, E. Jahn, M. Bülow, Zeolites 11 (1991) 308.
[32] K.J. Pike, S.E. Ashbrook, S. Wimperis, Chem. Phys. Lett. 345 (2001) 400–409.
[33] J.P. Amoureux, A. Flambard, L. Delevoye, L. Montagne, Chem. Commum. (2005) 3472–3474.
[34] Z. Gan, H.T. Kwak, J. Magn. Reson. 168 (2004) 346–351.
[35] T. Vosegaard, F.H. Larsen, H.J. Jakobsen, P.D. Ellis, N.C. Nielsen, J. Am. Chem. Soc. 119 (1997) 9055–9056.
[36] R. Lefort, J.W. Wiench, M. Pruski, J.P. Amoureux, J. Chem. Phys. 116–126 (2002) 2493–2501.